This manuscript is a non-peer reviewed preprint submitted to EarthArXiv. This manuscript is under review in Journal of Hydrometeorology.

How Will Precipitation Characteristics Associated with Tropical Cyclones in Diverse Synoptic Environments Respond to Climate Change?

Katherine E. Hollinger Beatty[a] , Gary M. Lackmann[a] , and Jared H. Bowden[a,b]

[a] *North Carolina State University, Raleigh, North Carolina*

[b] *North Carolina State Climate Office, Raleigh, North Carolina*

Corresponding author: Katherine E. Hollinger Beatty, kehollin@ncsu.edu

ABSTRACT: Landfalling tropical cyclones (TCs) can produce large rainfall totals which lead to devastating flooding, loss of life, and significant damage to infrastructure. Many studies have examined future changes in TC precipitation, however few have considered changes owing to differences in the synoptic environment during landfall. Here we focus on three North Atlantic TCs that impacted the southeastern United States: Hurricanes Floyd (1999), Matthew (2016), and Florence (2018). While these storms were impactful when they occurred, how might the impacts of similar systems change in a future climate? We address these questions using a Pseudo-Global Warming (PGW) approach and ensembles of convection-allowing numerical model simulations. With this method, we compare future changes in precipitation characteristics such as accumulated rainfall, and rain rate frequency and distribution to assess how these changes differ as a function of synoptic environment. Hurricanes Matthew and Floyd, which have more synoptic-scale forcing for ascent while over our study region, exhibit higher average rain rates in the present and future than the more tropical Hurricane Florence, but Florence exhibits the largest increases in rain rates ($34 \pm 12\%$ versus $23 \pm 9\%$ and $21 \pm 6\%$ for Hurricanes Matthew and Floyd, respectively). When we consider accumulated precipitation, Hurricanes Matthew and Floyd have larger areal increases in precipitation greater than 250 mm than Florence ($17600 \pm 800 km^2$ and $22400 \pm 400 km^2$ versus $9800 \pm 500 km^2$). These results point to the potential for future TCs in synoptically forced environments to have larger spatial footprints of heavy precipitation but smaller increases in rain rate than storms with less synoptic forcing, especially when considering over-land precipitation.

SIGNIFICANCE STATEMENT: Many previous studies demonstrate that tropical cyclone (TC) precipitation will increase in a warmer climate, but few studies consider how TC precipitation responds to climate change as a function of the accompanying weather pattern. Here, we examine future changes in precipitation for TCs in three distinct weather patterns. By analyzing the response of TC rainfall to warming for a diverse set of patterns, we can make recommendations for infrastructure and increase readiness for a variety of future scenarios, with the ultimate goal of maximizing the resilience of future transportation infrastructure. Specifically, rainfall output from these simulations is being used to stress test for future flooding risks with a current emphasis on long-lived transportation infrastructure in North Carolina.

1. Introduction

As tropical cyclones (TCs) affect coastlines and communities, they can cause substantial structural damage and loss of life. One of the largest contributors to these impacts is heavy precipitation and subsequent flooding or flash flooding. Rappaport (2014) found that for historical Atlantic TCs affecting the United States (US), approximately one quarter of the fatalities were a result of rain-induced flooding. When considering the frequency of fatalities, they found that nearly half of the TCs that resulted in at least one US fatality had a fatality due to rain-induced flooding (Rappaport 2014). This is especially true in the US states of North and South Carolina, where in the last 10 years, flooding from storms such as Hurricane Florence (2018) and Hurricane Matthew (2016) resulted in dozens of fatalities, multiple road washouts, and the closure of multiple major state and interstate highways (Stewart 2017; Stewart and Berg 2019). More recently, the damage to transportation infrastructure in western NC, and fatality counts in the hundreds in association with Hurricane Helene (2024) again underscores the importance of mitigating impacts.

It is clear that heavy rainfall from TCs has caused devastating impacts historically, and many previous studies have also examined how precipitation and its associated impacts may change as the climate warms. Per the IPCC AR6 Report (Seneviratne et al. 2023), there is high confidence that TC rain rates will increase in the future; for TCs passing over or near North Carolina, specifically, Kunkel et al. (2020) report that the heavy precipitation associated with them is very likely to increase. Of the numerous studies that have analyzed TC precipitation changes with climate change, a central finding is an increase in rain rates that either follows, or in some studies exceeds, the Clausius-Clapeyron scaling (~7% increase per degree Celsius of warming) (Knutson and Tuleya 2004; Hill and Lackmann 2011; Knutson et al. 2015). Knutson et al. (2020), in reviewing multiple studies, found that near-storm TC rain rates globally increase by a median value of 14% with a range from 6 to 22%, with slight variations by ocean basin, for a 2°C warming scenario; studies of the North Atlantic TCs show a median increase of ~16% (Knutson et al. 2020). While rainfall characteristics for TCs over water are important to understand, most of the societal impacts from TC rainfall, such as flooding, road washouts, and fatalities, occur once the storm is over land. A smaller portion of TC rainfall studies have focused explicitly on these landfalling/over-land changes in precipitation (Wright et al. 2015; Liu et al. 2018; Stansfield et al. 2020; Knutson et al. 2022), and their results are consistent in showing increased average post-landfall TC rain rates. While these studies provide useful insight, one limitation of many such studies is their use of lower-resolution simulations and datasets, and methods that do not capture the full extent of changes in TC intensity or precipitation (e.g. Liu et al. 2018; Stansfield et al. 2020).

When TCs make landfall or interact with land, especially once they enter the mid-latitudes, they often undergo the process of extratropical transition (ET) and some of their tropical features are replaced with extratropical characteristics. This phenomenon has been studied extensively (e.g. Jones et al. 2003; Evans et al. 2017; Keller et al. 2019), and its correlative changes in rainfall characteristics, including a shift of the heaviest precipitation into the northwest quadrant of the storm, are well understood (e.g. Atallah et al. 2007). How these extratropical transitioning storms will change with climate warming has also received recent attention (e.g. Liu et al. 2017; Michaelis and Lackmann 2019; Bieli et al. 2020; Liu et al. 2020; Michaelis and Lackmann 2021; Jung and Lackmann 2021, 2023), however only a few studies have focused specifically on rainfall, and how ET TC rainfall changes compare with non-ET TCs that are more tropical in character (e.g. Liu et al. 2018). Another factor that coincides with TCs in various life-cycle phases is the different synoptic environments within which they exist, and how the rainfall produced by TCs in distinct environments may change as the climate warms. To the authors' knowledge, this aspect, specifically, has received very limited attention.

Our goal in this paper is to focus on how TC rainfall over land changes with climate warming, and how these changes differ for TCs at various stages of their life cycle (tropical versus extratropical-transitioning) and in differing synoptic environments. To answer these questions, we analyze three synoptically diverse TCs that produced prolific rainfall (greater than 400 mm maximum accumulated rainfall) over the United States in North and South Carolina, specifically: Hurricanes Floyd (1999), Matthew (2016), and Florence (2018). We conducted ensemble simulations of these three storms at high-resolution using the Weather Research and Forecasting (WRF) model (Skamarock et al. 2021) for present-day conditions, and then in a future environment using a Pseudo-Global Warming (PGW, a.k.a. physical climate storyline) approach (Schär et al. 1996; Frei et al. 1998; Kimura and Kitoh 2007; Sato et al. 2007; Baulenas et al. 2023). This approach has proven successful for various precipitation-producing weather phenomena previously, including individual TCs (e.g. Lackmann 2015; Jung and Lackmann 2019; Carroll-Smith et al. 2020; Reed et al. 2020), full TC seasons (e.g. Mallard et al. 2013a,b; Gutmann et al. 2018), and smaller-scale convective systems (e.g. Lackmann 2013; Trapp and Hoogewind 2016; Dougherty and Rasmussen 2020; Dougherty et al. 2023). Along with understanding how the rainfall will change, these simulations are also being used as future "design storms" by the North Carolina Department of Transportation (NCDOT) to stress test highway infrastructure using 2D hydraulic models. Insight provided by these models about plausible future flooding is then being used to inform climate change adaptation decisions.

This paper focuses on how the precipitation characteristics for these storms responds to climate change. Section two focuses on data and methods, followed by an evaluation of the simulations with respect to observations in section three. Section four discusses specific changes in precipitation characteristics for these storms, including changes in accumulated precipitation, rain rate distribution, and rain rate spatial extent, followed by conclusions and discussion in section five.

2. Data and Methods

a. Case selection and overview

For this study, we chose to analyze Western North Atlantic Hurricanes Matthew (2016), Florence (2018), and Floyd (1999) with a specific focus on the portion of their lifetime as they approached and impacted the US states of North and South Carolina. We selected these cases on the basis of their contrasting synoptic environments, which influenced the track (Fig. 1), structure, and evolution of these systems: one remained more purely tropical (Florence) and two underwent ET but followed drastically different track evolutions and experienced different amounts of environmental vertical wind shear (Floyd and Matthew). These cases are also of interest to the NCDOT because they each resulted in extensive disruption and damage to transportation infrastructure, in addition to being responsible for numerous fatalities. Hurricanes Matthew and Florence in particular resulted in the closure of multiple major interstate highways. While these storms do not represent all possible storm evolutions that could impact this region, they provide diverse synoptic representations of impactful storms in this region.

Hurricane Matthew briefly made landfall in northeastern South Carolina near McClellanville around 1500 UTC 8 October 2016 before making a sharp eastward turn as it interacted with an eroding subtropical high and an approaching mid-latitude trough (Stewart 2017). Because of the interactions with the approaching trough and an existing front over North Carolina, Hurricane Matthew's cloud and precipitation shield was shifted to the northwest of the storm center, resulting in large regions of greater than 250 mm (10 inches) of rain over central and eastern NC, with a maximum measured value of 481 mm (18.95 inches) reported near Evergreen, NC (Fig. 2a) (Stewart 2017). This left-of-track precipitation shield, which was influenced by an existing front and increasing southwesterly shear from an approaching trough, is similar to what was seen with Hurricane Floyd, though the tracks for these two storms differed substantially (Figs.1, 2a,c). It is also indicative of a shift to an asymmetric warm-core system instead of a more tropical symmetric warm core TC (Fig. 3a). After impacting North Carolina, Matthew continued to move eastward over the Atlantic before fully losing its tropical characteristics around 1200 UTC 9 October, then merging with the frontal system by 0000 UTC 10 October (Stewart 2017).

Hurricane Florence made landfall near Wrightsville Beach, NC as a category one hurricane around 1115 UTC on 14 September 2018 (Stewart and Berg 2019). As it approached North Carolina from the east-southeast, its steering flow weakened, which caused a subsequent decrease in translation speed. This slow translation speed allowed for continued onshore flow of warm, moist air from over the warm Gulf Stream waters off the coast of the Carolinas, resulting in multiple rain bands passing over the same parts of southeastern North Carolina and prolonging the duration of heavy precipitation. There were large regions of greater than 250 mm (10 inches) of rainfall in central and southeastern North Carolina, with a smaller region of greater than 500 mm (20 inches) over far southeastern NC, and a localized region of greater than 750 mm (30 inches) from the persistent rain bands; the peak rainfall reported was 912 mm (35.93 inches) near Elizabethtown,

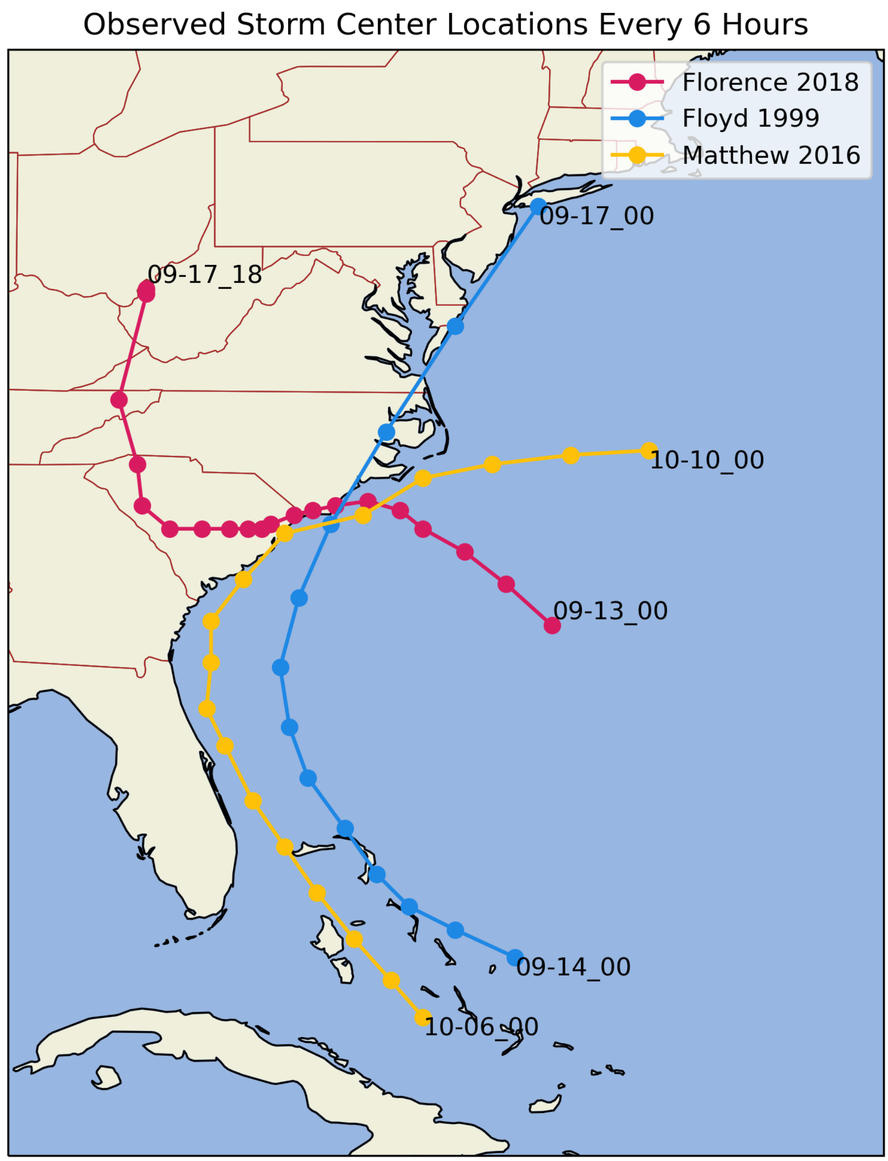

Figure 1. Observed National Hurricane Center (NHC) second-generation hurricane database (HURDAT2; Landsea and Franklin 2013) storm tracks of Hurricanes Matthew (2016), Florence (2018), and Floyd (1999) during the portion of their life cycles when they were approaching or affecting the study area. The times plotted for these tracks align with the start and end times of our model simulations. Numbers correspond to month-day-hour in UTC and dots represent 6-hourly center positions.

NC (Fig. 2b) (Stewart and Berg 2019). Because of its slow translation speed, Florence continued to produce heavy rainfall over some parts of central and eastern North Carolina for over 72 hours, and maintained symmetric warm core tropical characteristics until it reached West Virginia around

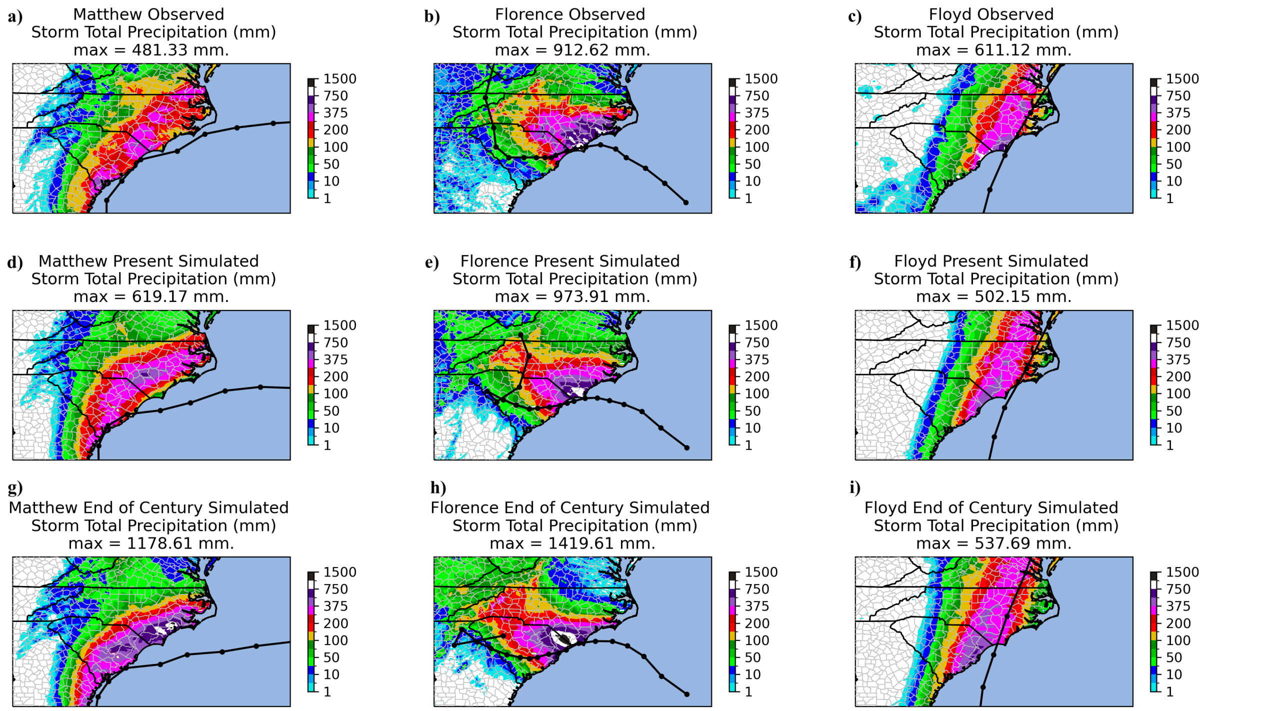

Figure 2. Precipitation and track summary, panels (a)-(c): Black line is observed NHC best track for Hurricanes (a) Matthew (2016), (b) Florence (2018), and (c) Floyd (1999) with storm total precipitation (shaded, mm as in legend at right). Observed precipitation for Hurricanes Matthew and Florence is Stage IV and for Hurricane Floyd is Livneh daily CONUS near-surface gridded precipitation provided by the NOAA PSL (Livneh et al. 2013). Panels (d)-(f): Simulated ensemble mean track and probability matched mean total accumulated precipitation (mm) from WRF model simulations of Hurricanes (d) Matthew, (e) Florence, and (f) Floyd. Panels (g)-(i): ensemble mean track and probability matched mean total accumulated precipitation (mm) from future WRF model runs of Hurricanes (g) Matthew, (h) Florence, and (i) Floyd.

1200 UTC 17 September when it was officially considered extratropical (Stewart and Berg 2019, Fig. 3b).

Hurricane Floyd made landfall near Cape Fear, North Carolina at 0630 UTC on 16 September 1999 as a category two hurricane on the Saffir-Simpson scale (Pasch et al. 1999). In the roughly 24 hours that Floyd directly affected the Carolinas, it produced large regions of 250-400 mm (10-15 inches) of rain, with a peak value of 611 mm (24.06 inches) reported near the coast in Wilmington, NC (Fig. 2c) (Pasch et al. 1999). This rainfall was likely enhanced by Floyd's interactions with an approaching cold front and upper-tropospheric trough (Atallah and Bosart 2003). As Floyd

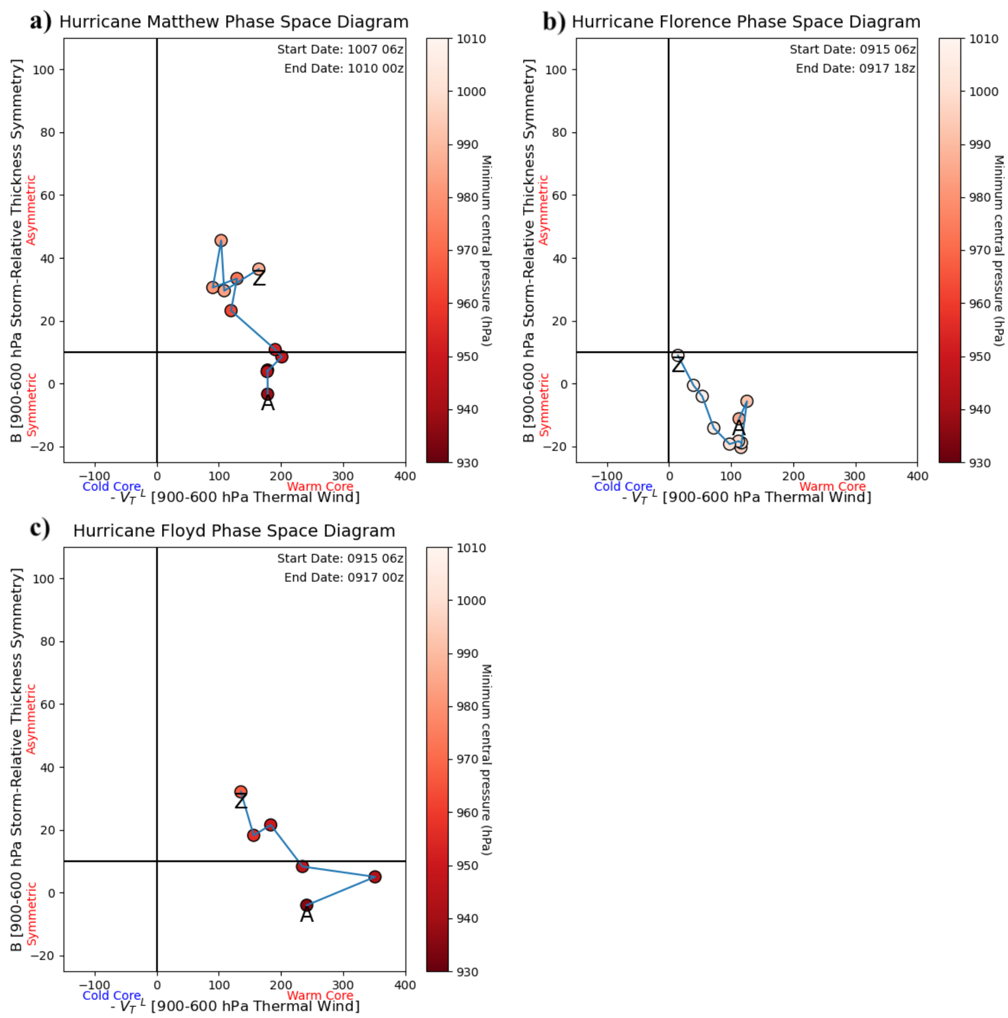

Figure 3. Cyclone phase space (CPS) diagrams of thickness symmetry versus lower-tropospheric thermal wind for Hurricanes Matthew (a), Florence (b), and Floyd (c). The B and VLT variables are calculated every 6 hours from ERA5 reanalysis data valid at that time, and the minimum central pressure data is from HURDAT2. The values are plotted every 6 hours with color shading to indicate the minimum central pressure (hPa) for each storm as in legend at right. The letters A and Z represent the beginning and end of time window for each storm listed in the upper right of each plot, respectively. These times are a subset of the times plotted for the tracks in Figure 1.

approached and moved across North Carolina, its translation speed increased. It then turned north-northeast and encountered an environment with increased south-southwesterly shear, and began to acquire extratropical characteristics which classified it as an asymmetric warm core system (Fig. 3c). Floyd moved up the East Coast and continued to interact with the front, producing rainfall totals greater than 250 mm across Maryland, Delaware, and New Jersey and record breaking rainfall in Philadelphia (Pasch et al. 1999). It was classified as a frontal low by the time it reached Maine, thus completing its extratropical transition. See Atallah and Bosart (2003) and Colle (2003) for a thorough analysis of Hurricane Floyd's life cycle and extratropical transition along the US East Coast.

b. Model configuration

We simulated each storm using the Weather Research and Forecasting (WRF) Model version 4.2.2 (Skamarock et al. 2021). We experimented with different initialization (and lateral boundary condition) datasets to identify which yielded simulations that most closely matched observations. We decided to initialize Hurricane Matthew with the 0.25° ERA5 dataset (Hersbach et al. 2020) and simulated the period from 00 UTC 06 October until 00 UTC 10 October 2016. For Hurricane Florence, we used the 0.25° Final Global Data Assimilation System (GDAS/FNL) dataset (National Centers for Environmental Prediction, National Weather Service, NOAA, U.S. Department of Commerce 2015) and simulated the period from 00 UTC 13 September until 18 UTC 17 September 2018. For Hurricane Floyd, we used the 0.5° Climate Forecast System Reanalysis (CFSR) (Saha et al. 2010) dataset and simulated the period from 00 UTC 14 September to 00 UTC 17 September 1999. We selected these initial condition data for each case in order to optimize the representation of TC track and precipitation over the study area. We ran a mini-ensemble of simulations for each storm based on varying physical parameterizations; this ensures that results are not particular to a specific set of model physics choices, and offers a more robust solution, while also providing ensemble statistics and information about uncertainty. For Hurricane Matthew, we ran six ensemble members while for Hurricanes Florence and Floyd we ran seven ensemble members. The full list of the key physics choices made in each ensemble member is listed in Table 1. Each of our storms had a parent domain with 12-km grid spacing and a stationary inner nest with 4-km grid spacing (Fig. 4); we used two-way nesting so that information from the high-resolution domain was fed

Table 1. Physics choices used for each ensemble member for WRF simulations. Hurricanes Florence and Floyd used all 7 members, while Hurricane Matthew only used the first 6.

	$Member1$	$Member2$	$Member3$	$Member4$	$Member5$	$Member6$	$Member7$
Microphysics	Thompson	WSM6	Thompson	Goddard	P3	WDM6	WDM7
Cumulus (domain 1 only)	Tiedtke	Tiedtke	BMJ	Tiedtke	Tiedtke	Tiedtke	Tiedtke
PBL	YSU	YSU	MYJ	YSU	YSU	YSU	YSU
Surface-layer	MM5	MM5	Eta	MM5	MM5	MM5	MM5
Shortwave Radiation	RRTMG	RRTMG	RRTMG	RRTMG	RRTMG	RRTMG	RRTMG
Longwave Radiation	RRTMG	RRTMG	RRTMG	RRTMG	RRTMG	RRTMG	RRTMG

back to the parent domain. The physics choices for each ensemble member are the same for both the parent domain and the nest, with the exception of the cumulus scheme which was turned off for the nested domain given the higher resolution. All ensemble members also used the ocean mixed layer model to adjust for the cold wakes behind the TCs and the "isftcflx" in WRF is set to the Donelan/Garret formulation to adjust the overwater surface flux exchange coefficients at high wind speed (Donelan et al. 2004).

Given that the focus of our study is over-land precipitation and how it responds to climate change, it is imperative that our present and future storms overlap as much as possible; as such, the simulation verification metric we emphasize is the accumulated storm-total rainfall. To maintain track similarity and more similar accumulated rainfall distributions, we used spectral nudging for each ensemble member for Hurricanes Matthew and Florence (Waldron et al. 1996; von Storch et al. 2000; Bowden et al. 2012; Otte et al. 2012). Our specific configuration included nudging of only the winds above the boundary layer (model level 10 which corresponds to ~800 hPa base state pressure) at wavenumbers three and smaller on the parent domain; this corresponds to features at spatial scales on the order of 1000 km and greater. We did not nudge geopotential, temperature, or water vapor, and we did not nudge any variables in the nested domain. Our goal with this configuration was to nudge just the large-scale pattern to the reanalysis data to allow the steering flow to be similar in the present and future environments while still allowing the storm-scale features to evolve as freely as possible, and to maintain the warmer thermodynamic conditions for the future simulations. While we tested nudging with Hurricane Floyd, we ultimately did not use

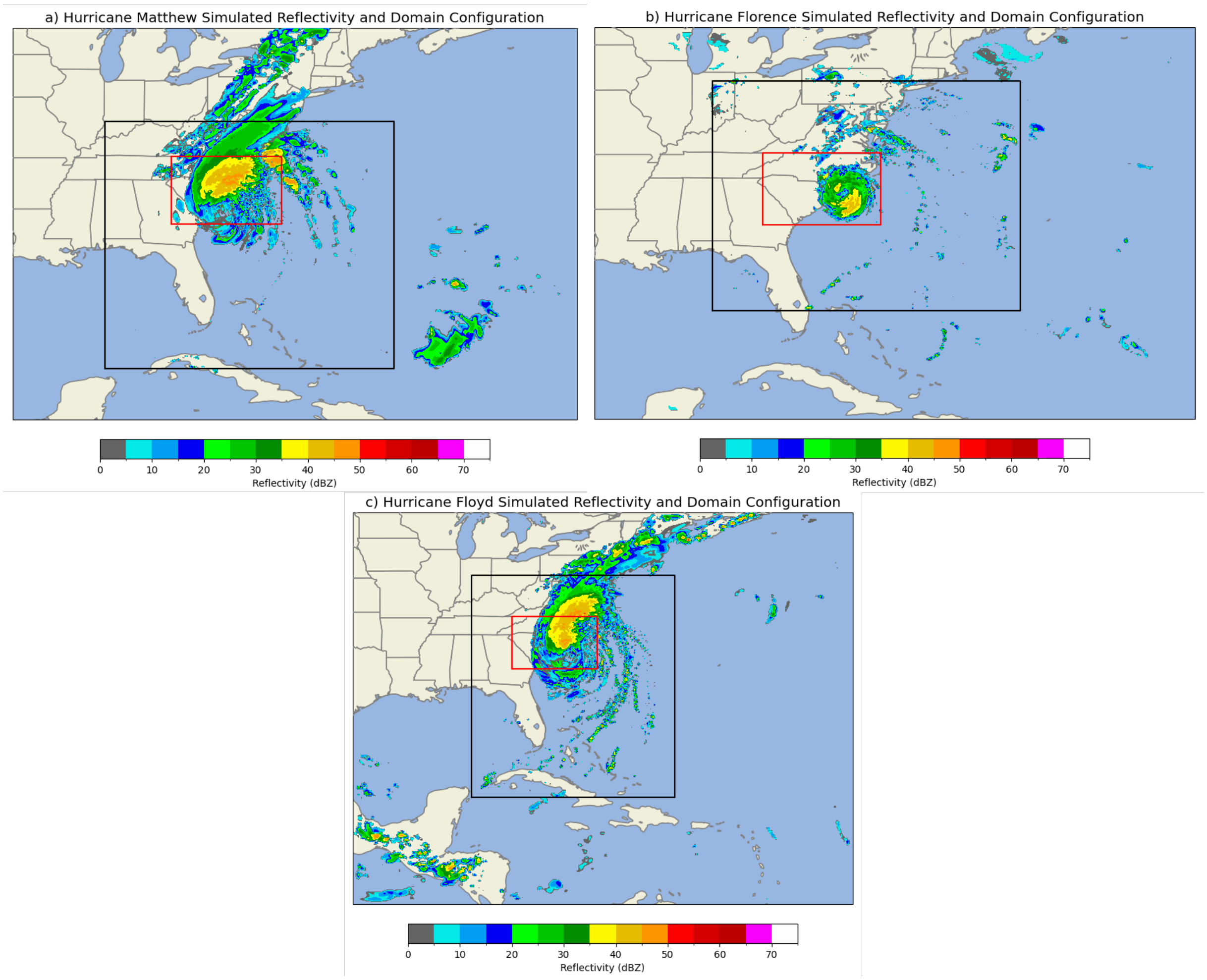

Figure 4. WRF domain configurations for Hurricanes Matthew (a), Florence (b), and Floyd (c). The full image is the 12 km parent domain and the black box is the 4 km nested domain. The red box represents the averaging domain used when considering rainfall changes over the Carolinas. The simulated reflectivity is valid at 18z 08 October, 12z 14 September, and 06z 16 September for Hurricanes Matthew, Florence, and Floyd, respectively, and at 12km and 4km resolution in each respective domain.

it because the tracks were sufficiently similar to observations without nudging (Fig. 5c,f). We recognize that nudging limits modification of the future TC environment.

In order to compensate for large underestimations in TC intensity in available reanalyses for Hurricane Floyd, we initialized simulations of that storm with a synthetic vortex, following Nolan et al. (2021). This method allowed the intensity of the storm to be closer to observations relative to simulations initialized with the reanalysis alone. The synthetic vortex was especially useful for

Hurricane Floyd, but was not used for Matthew or Florence. For Florence, the intensity, track, and precipitation distribution using reanalysis alone aligned well with the observations (discussed in section 3), so the vortex was not needed. For Matthew, the precipitation distribution and the tracks were close to observations without the synthetic vortex, however the intensity was substantially weaker than observed. To attempt to resolve this disparity, we tested one ensemble member using the synthetic vortex, and while the intensity improved, the storm track and precipitation distribution were more poorly represented (not shown). Given the purpose of these simulations for assessing transportation risk to hurricane precipitation in a warmer climate, the non-synthetic vortex Matthew runs were sufficient. Throughout the model configuration process, all simulations were compared with their respective storm's observed track, intensity, and precipitation distribution to assess their validity, which will be discussed in more detail in section three. The differences between each of the storm simulation configurations are displayed in Table 2.

c. Future climate simulations

To investigate how these storms would differ in a future thermodynamic environment, we used a PGW approach (Schär et al. 1996; Frei et al. 1998; Kimura and Kitoh 2007; Sato et al. 2007) as has been done successfully in numerous previous studies (e.g. Mallard et al. 2013a,b; Lackmann 2013, 2015; Trapp and Hoogewind 2016; Gutmann et al. 2018; Jung and Lackmann 2019; Carroll-Smith et al. 2020; Dougherty and Rasmussen 2020; Dougherty et al. 2023). After evaluating our present-day simulations against observations (see section three), we then simulated each storm with projected end-of-century conditions. To accomplish this, we calculated 20-year difference fields ("deltas") for five different temperature variables (skin temperature, surface temperature, soil temperature, air temperature, and sea-surface temperature) using an ensemble of Phase 5 Coupled Model Intercomparison Project (CMIP5) or CMIP6 models using the Representative Concentration Pathways (RCP) 8.5 or Shared Socioeconomic Pathway (SSP) 5-8.5 emissions scenarios (Moss et al. 2010; Gidden et al. 2019). These scenarios were chosen to assist the NCDOT in understanding climate change flooding risks and vulnerabilities when planning long-lived, resilient transportation infrastructure. We also hold relative humidity constant, which, with warming, results in a moisture delta that is consistent for present-day and future environments. The final step is the WRF preprocessing interpolation that recalculates geopotential height and ensures hydrostatic balance

Table 2. Description of the varying options and configurations for each storm.

	Hurricane Matthew	*Hurricane Florence*	*Hurricane Floyd*
Initial and lateral BCs	ERA5	GDAS	CFSR
Vortex initialization?	no	no	yes
Spectral nudging of winds?	yes	yes	no
Number of ensemble members	6	7	7
CMIP data	CMIP5	CMIP6	CMIP5

with the new virtual temperature field. For both present and future simulations, we use digital filter initialization (DFI) (Lynch and Huang 1992; Peckham et al. 2016) to minimize high frequency noise that may occur in the model as a result of thermodynamic changes, and to generate hydrometeor and cloud fields for the initial model time, reducing the need for long model spin-up time.

For Hurricanes Matthew and Floyd, we calculated deltas using an ensemble of 20 CMIP5 models for a future time period of 2080-2099 minus a historical time period of 1980-1999. This results in a 100-year temperature delta. For Hurricane Florence, we instead calculated deltas using an ensemble of 20 CMIP6 models for a future time period of 2080-2099 and a historical time period of 1995-2014, which results in an 85 year delta. We explicitly calculate these deltas by averaging each variable over the respective time periods and across all of the chosen models, then subtracting the two time periods (future and historical). These deltas are then applied to their respective temperature variables in the WRF initialization files to represent thermodynamic environments that are 100, 85, and 100 years after the storms originally occurred for Hurricanes Matthew, Florence, and Floyd, respectively. There is not a distinguishable difference in the time- and ensemble-averaged projected future temperature in our study region between CMIP5 and CMIP6 ensembles (not shown). The list of CMIP5 models we used is the same as those used in Jung and Lackmann (2019), and the CMIP6 models we used are listed in Table 3. Six of these models have equilibrium climate sensitivity (ECS) values above 4.5 degrees Celsius, categorizing them as "hot models" (Tokarska et al. 2020; Hausfather et al. 2022).

d. Return period quantification

Given larger projected changes in extreme storms in the future with additional atmospheric warming (Seneviratne et al. 2023), it is important to investigate climate change projections and

Table 3. List of CMIP6 models used to compute change fields used in Hurricane Florence PGW simulations. All models utilized the SSP 5-8.5 scenario.

Models		
ACCESS-CM2	ACCESS-ESM1-5	BCC-CSM2-MR
CAMS-CSM1-0	CanESM5	CESM2
CESM2-WACCM	CMCC-ESM2	CNRM-CM6-1
EC-Earth3	FGOALS-g3	GISS-E2-1-G
IPSL-CM6A-LR	MIROC6	MPI-ESM1-2-HR
MPI-ESM1-2-LR	MRI-ESM2-0	NorESM2-LM
NorESM2-MM	TaiESM1	

the issue of non-stationary within readily available climate information especially as it relates to precipitation extremes. In particular, there is growing interest in precipitation changes and how these changes may impact hydrologic design (Wright et al. 2019; Kourtis and Tsihrintzis 2022). Hydrologic design standards in North Carolina (NC) and throughout a majority of the US use existing intensity-duration-frequency (IDF) curves (NOAA Atlas 14; Bonnin et al. 2004); however, these curves do not consider non-stationarity and climate change.

Here we put the simulated hurricanes (now and future) in the context of NOAA Atlas 14 and a scaled version of Atlas 14 for NC (Bowden et al. 2024, 2025) that considers plausible changes using downscaled climate change projections from the Localized Constructed Analogs dataset (LOCA; Pierce et al. 2014). This method creates a regional scale factor for the eight climate divisions in NC for each General Circulation Model (GCM), different return periods, greenhouse gas emission scenarios, and time horizons of concern defined by NCDOT. An ensemble of all downscaled GCM scale factors is created and applied to adjust Atlas 14. Scaling Atlas 14 is noted as a viable option (Kilgore et al. 2019) with scale factors developed for other regions using downscaled climate change projections, similar to the work presented by Miro et al. (2021) for the US Mid-Atlantic region. An assumption is made to estimate the sub-daily rainfall accumulations and intensities using the 24-hr regional scale factors. The historical and projected changes in the scaled IDF values are compared with the simulated hurricanes to begin investigating non-stationarity in the future IDF curves.

To calculate the return periods for our simulated storms, we store the highest 100 precipitation values at nested domain grid cells for the six thresholds from each ensemble member: 1-hr, 2-hr, 3-hr, 6-hr, 12-hr, and 24-hr. Then, we calculate the mean and standard deviation of the stored data for each time interval. For comparison, observed NOAA Atlas 14 values were selected for the location in eastern North Carolina with the highest return period values, New Hanover County. We chose the observed maximum IDF values in the region because the events we are simulating are extreme. The future (scaled) IDF values for end-century and the same high-emission scenario for the centroid county estimate are used to estimate projected rainfall for the different durations and return periods.

3. Model storm simulation performance

a. Present day simulations compared with observations

Each ensemble mean storm track aligns fairly well with the observed tracks, with the root mean square deviation (RMSD) for each storm's center falling within 130 km of the observed location. For the simulated tracks, we define the TC center location as the location on the 4-km WRF nest with the lowest sea level pressure. Of the three storms, the ensemble mean for Floyd has the largest RMSD due to the simulated storm traveling slower than observed after exiting the Carolinas. Visually, Hurricane Matthew appears to exhibit the largest track error, though its RMSD is only ~75 km due to the storm deviating to the west of the observed track, especially at the beginning of the simulation. We explored several options to improve this issue (not shown here); the configuration presented here represents a combination of the best simulated track and precipitation distribution compared to observations. The ensemble mean track for Hurricane Florence was similar to the observed, consistent with smaller quantitative track errors (Table 4).

The intensity for the present-day simulations was more difficult to align with observations, particularly for Hurricane Matthew. The large discrepancy in intensity with Hurricane Matthew is expected, based on the more westward track in the simulations that resulted in greater land interaction relative to observations, as well as the reanalysis representation of the intensity being too weak. The RMSD of the ensemble mean central pressure for Matthew is too high by ~21-hPa (Table 4). While this is a large difference, the precipitation values over North and South Carolina still compared well with observations (Fig. 2a,d). Given that the precipitation from Hurricane

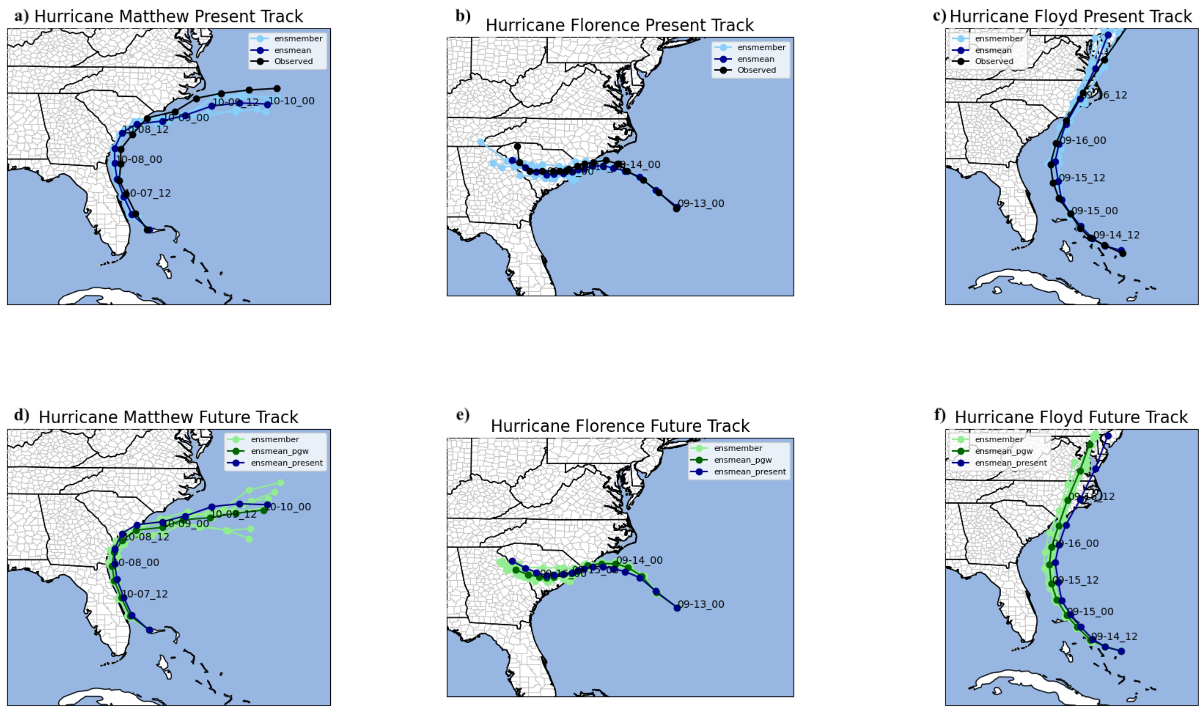

Figure 5. Ensemble storm tracks of Hurricanes Matthew (a,d), Florence (b,e), and Floyd (c,f), ensemble mean, and observed NHC track. Present-day simulations are in panels a-c and future simulations d-f. The black line represents the NHC best track, the lighter blue (green) lines represent ensemble members, and the darker blue (green) represents the ensemble mean for the present (future) storms. The extent of the figures represents the size of the high-resolution nested domain for each storm simulation.

Matthew was influenced by an approaching upper-level trough and a lower-tropospheric stationary front, as opposed to tropical cyclone processes alone, we accepted the intensity error in these simulations. Simulated intensities for Hurricanes Floyd and Florence aligned much better with observations, with error values of only ~5 and ~7-hPa, respectively (Table 4).

As mentioned above, an important metric we used to ensure the adequacy of our runs was the similarity between the observed and modeled total accumulated precipitation for each storm (Fig. 2a-f). We subjectively analyzed each storm's simulated ensemble probability matched mean accumulated precipitation and compared its spatial footprint and maximum precipitation amounts with the Stage IV precipitation analysis for Hurricanes Matthew and Florence, and Livneh (Livneh et al. 2013) precipitation for Hurricane Floyd. Overall, the spatial footprint of the accumulated precipitation aligns well for all of our storms, but the grid-cell maximum storm total precipitation

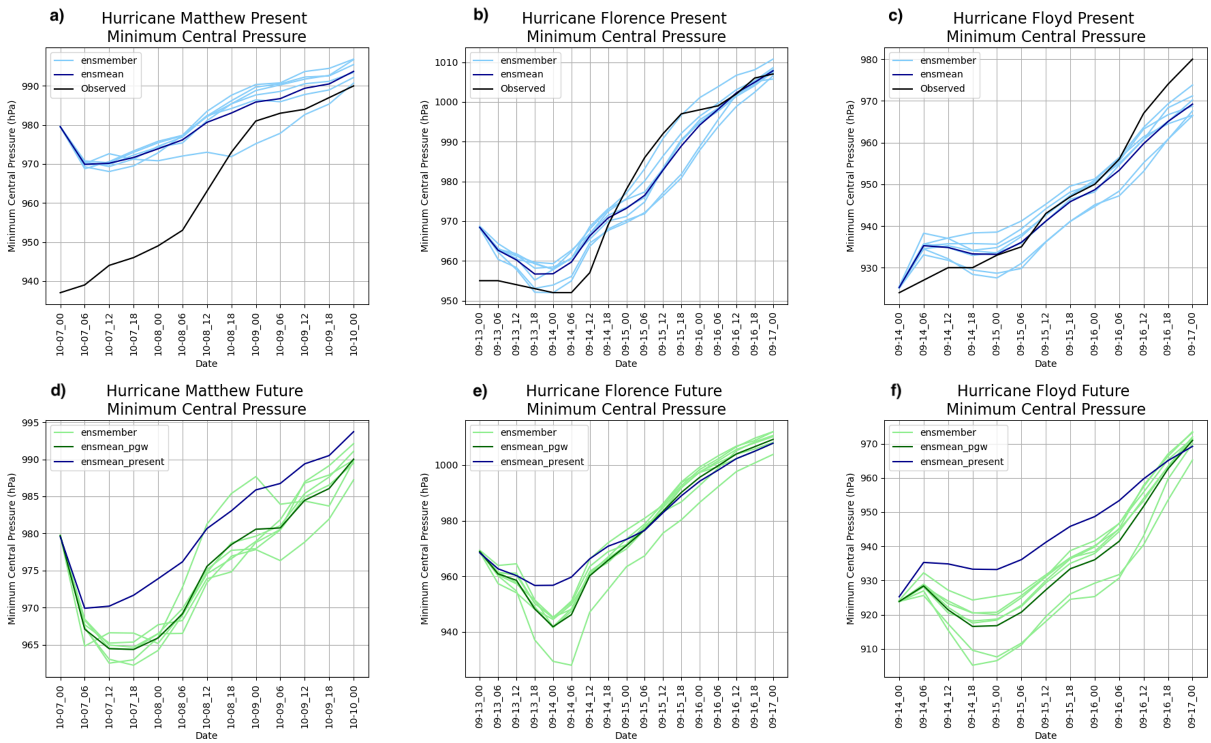

Figure 6. TC central pressure for Matthew (a, d), Florence (b, e), and Floyd (c, f). Top row is present (with NHC best track in black) and bottom row is future ensembles. Thin lines are ensemble members and darker colored line is ensemble mean.

differs by over 100 mm for Hurricanes Matthew and Floyd (Figure 2). Considering the track, intensity, and precipitation similarities, we deemed the ensemble simulations sufficient to proceed with analysis.

b. Present day compared with future simulations

Comparing the resulting present-day and future ensemble mean storm tracks, we find that, as expected, they are quite similar for all storms (Fig. 5). While subtle track differences do exist with each storm, overall their tracks are sufficiently similar to allow for precipitation comparisons, especially given that many of the comparisons will be done via an averaging box over North and South Carolina land points (Fig. 4). For each of our storms, the future ensemble mean track falls within a reasonable distance from the present ensemble mean, with the RMSD track difference for Matthew and Florence being less than 40 km, and for Floyd less than 60 km (Table 4).

Table 4. Track and intensity comparison summary. Great-circle distances RMSD (km) are shown in column one, while the storm minimum sea-level pressure RMSD (hPa) is shown in column two. Rows one through three compare observed values (NHC best track) with simulated present ensemble mean values (simulated minus observed), and rows four through six compare present-day ensemble mean values with future ensemble mean values for each storm (present minus future). Differences are calculated every six hours and averaged across all model times (13 times for Floyd and Matthew, 16 for Florence).

	Avg track RMSD (km)	*Avg minimum central pressure RMSD (hPa)*
Matthew Present to Observations	75.7	21.1
Florence Present to Observations	29.3	6.8
Floyd Present to Observations	126.3	4.9
Matthew Present to Future	38.6	5.4
Florence Present to Future	37.1	5.9
Floyd Present to Future	59.6	11.6

The future simulations for all storms reach lower ensemble mean minimum central pressures than their respective present-day counterparts (Fig. 6). The largest intensity increase occurs with Hurricane Floyd, which, at its highest intensity, features a minimum central pressure that is 17-hPa lower in the future ensemble mean relative to the present-day simulations of Floyd. The time-average difference between the present and future ensemble mean minimum central pressure shows that the largest difference also exists for Hurricane Floyd, which has a 12-hPa time-averaged difference (Table 4).

4. Changes in precipitation characteristics

a. Total accumulated precipitation

Several TC rainfall metrics can be used to quantify the complete nature of TC precipitation change between present-day and future simulations. One such metric is the total amount of precipitation that a system produces over land, for example, total accumulated rainfall at all land grid cells (Fig. 2). In the PGW simulations, the tracks deviate slightly, resulting in an associated shift of the precipitation swath which can complicate using a direct grid-cell difference between the present and future accumulated precipitation. However, we can still visually see an expansion of the 375-mm isohyet (~15 in) in all three cases (Fig. 2). Examining a variety of thresholds, we see an increase in the area receiving greater than 250, 375, 500, and 750 mm of accumulated rainfall in all future cases where those thresholds are met (Table 5). The largest areal increase for Floyd occurred where precipitation totals exceeded 250 mm ($22400 \pm 400 km^2$), for Matthew where precipitation totals exceeded 375 mm ($27000 \pm 500 km^2$), and for Florence where precipitation totals exceeded 375 mm ($9900 \pm 400 km^2$). Amongst the three storms, we see the largest areal increase in precipitation for any threshold above 250 mm in Hurricane Matthew ($27000 \pm 500 km^2$ for areas receiving greater than 375 mm). Hurricane Florence's largest areal increase for any threshold is less than Matthew and Floyd's largest changes by about half, indicating it had the smallest changes in footprint for high accumulated precipitation amounts (Table 5). Analyzing the change in the maximum accumulated precipitation value for a single grid cell over the Carolinas, we also found an increase for all storms, though the range is quite large between the three storms (+7% for Floyd, +90% for Matthew, and +46% for Florence) (not shown).

Most studies that evaluate TC rainfall and climate change report their percent changes as an average over a large area, making it difficult to compare when considering a smaller region. However, Wright et al. (2015) found that for North and South Carolina, when comparing rainfall for present-day TCs with future projections from CMIP3, early CMIP5, and late CMIP5, the spatial map of percent changes in rainfall show increased values ranging from 50 to 150% across our study region. This is quite similar to what we find here with localized regions of over 100% increases in accumulated rainfall for all three storms in parts of North and South Carolina (not shown), and average changes ranging from 40-130% across all three storms (Table 5). It is important to note,

Table 5. Change in the over-land area receiving rainfall thresholds of greater than 10 in (250 mm), 15 in (375 mm), 20 in (500 mm), and 30 in (750 mm), plus or minus the standard deviation. Also shown are the average percent change in total area receiving rainfall for regions only over land as well as over the land and ocean.

	Matthew (2016)	*Florence* (2018)	*Floyd* (1999)
250 mm.	$17600 \pm 800 km^2$	$9800 \pm 500 km^2$	$22400 \pm 400 km^2$
375 mm.	$27000 \pm 500 km^2$	$9900 \pm 400 km^2$	$9900 \pm 300 km^2$
500 mm.	$14000 \pm 100 km^2$	$9000 \pm 500 km^2$	$1300 \pm 100 km^2$
750 mm.	$2200 \pm 100 km^2$	$4600 \pm 300 km^2$	—
average change over our study region (land only)	+14%	+36%	+110%
average change over our study region (including ocean)	+68%	+40%	+130%

however, that in our study we use RCP8.5 and Wright et al. (2015) used RCP4.5/A1B. Liu et al. (2018) also evaluated how eastern US landfalling TC rainfall would evolve with climate change, and in doing so found that for landfalling TCs between July and November, the increase in rainfall over North and South Carolina ranged from 0-50% for the RCP4.5 future scenario. The large differences between their study and ours may be due in part to their model resolution being much coarser than ours (50-km grid spacing compared to 4-km), and their use of RCP4.5 instead of RCP8.5. Our results are also for three specific, extreme cases as compared to years-long composites of multiple storms. Jalowska et al. (2021), which evaluated the same three storms, found 22-44% increases in total rainfall across a similar study region based on end-of-century RCP4.5 and RCP8.5 warming. The dampened increases compared to what we find are not entirely surprising given their data is 36 km resolution compared to 4 km.

b. Distribution of rain rates

An important precipitation characteristic is the distribution of over-land rain rates for each of the storms, and how those distributions change in a warmer climate (Fig. 7). All three storms exhibit a decrease in the frequency of weaker rain rates (less than 12 mm per hour) and an increase in rain rates greater than 25 mm per hour, with Florence and Floyd showing future increases at all rain rates above 12 mm per hour. The biggest future increase in the occurrence of a given rain rate varies by storm, with Matthew having the largest increase around 30 to 33 mm (1.2 to 1.3 inches) per hour, Florence having the largest increase around 20 to 23 mm (0.8 to 0.9 inches) per hour, and Floyd having the largest increase around the 12 to 15 mm (0.5 to 0.6 inches) per hour range, when only considering rain rates above 12 mm per hour. The overall pattern of a decrease in the frequency of lower rain rates and increase in the frequency of higher rain rates aligns with previous studies (Lackmann 2013; Gutmann et al. 2018), and also points to the potential for our future storms to have higher flash-flooding potential than their present-day counterparts. A subsequent paper will explore the causes for this change in rain rate distribution.

As mentioned previously, a central finding of studies that examine changes in TC precipitation is an increase in rainfall that either follows or exceeds the Clausius-Clapeyron (CC) scaling (~7% increase per degree Celsius of warming) (Knutson and Tuleya 2004; Hill and Lackmann 2011; Knutson et al. 2015). For all of our simulations, the average temperature increase across the lower and middle atmosphere (surface to 500 hPa) from present to future was ~4.5K (Table 6). This temperature increase implies a vapor increase of ~35% for all storms. When we calculate the percentage change in precipitable water (PWAT), we find that all three storms have PWAT increases slightly under the expected vapor increase given by the CC scaling - these variations are understandable given that we averaged the 4.5K temperature change across height and location. Comparing the average rain rates from the histograms, we find percent increases of $23 \pm 9\%$, $34 \pm 12\%$, and $21 \pm 6\%$ for Hurricanes Matthew, Florence, and Floyd respectively (Table 6), which are sub-CC scale, CC scale, and sub-CC scale, respectively. When we consider the changes in the 90th percentile of these distributions, or the more extreme rain rates, we find increases of $37 \pm 7\%$, $55 \pm 20\%$, and $25 \pm 8\%$ for Hurricanes Matthew, Florence, and Floyd respectively (Table 6), which are CC scale, super-CC scale, and sub-CC scale respectively. For all three storms, this implies that the extreme precipitation rates are increasing more than the averages.

c. Areal extent of rain rates

While the frequency of rain rate occurrences is valuable, it is also important to see where these rain rates occur to determine if the spatial extent of heavy rain rates changes along with the

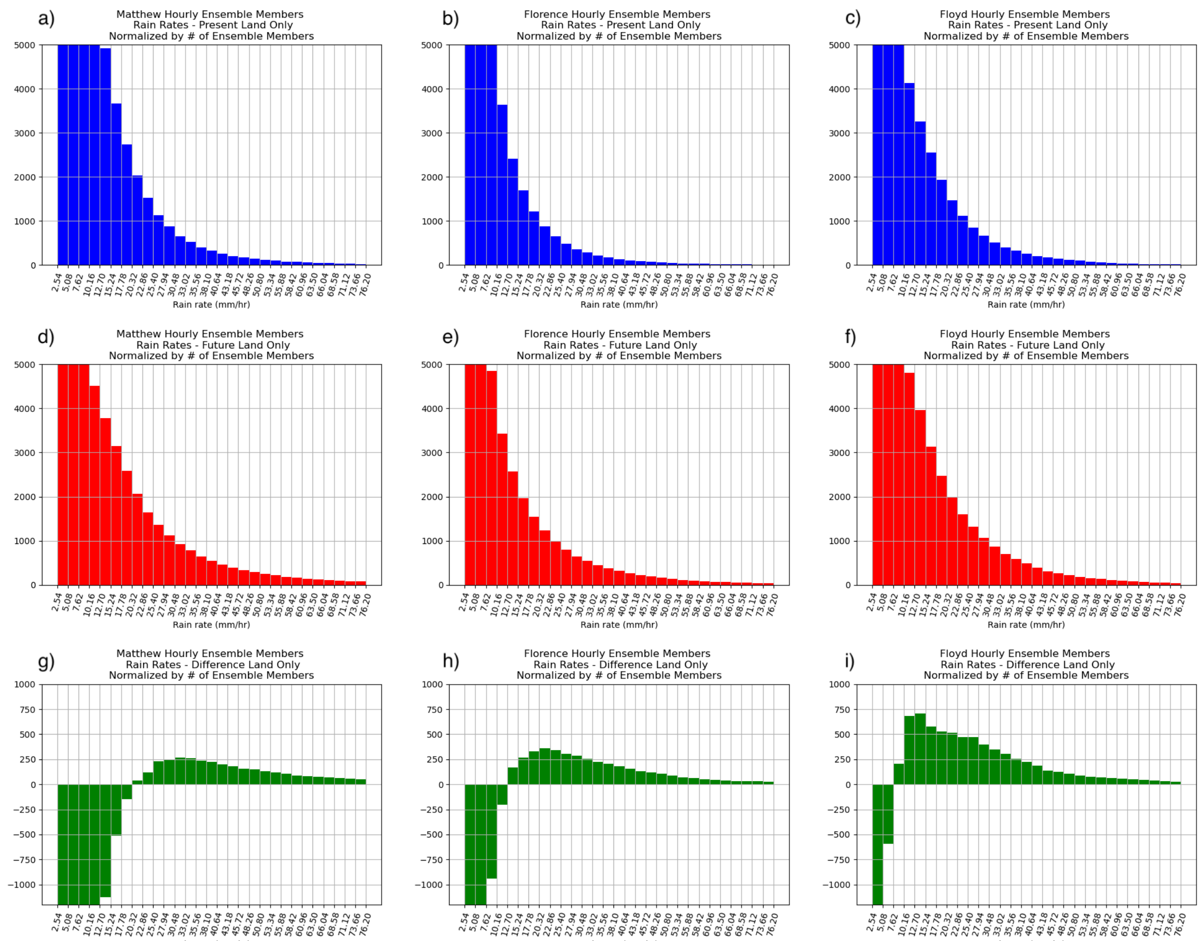

Figure 7. Histograms of ensemble mean rain rate (mm h^{-1}) for Hurricanes Matthew (a,d,g), Florence (b,e,h), and Floyd (c,f,i). Here we plot rain rates from present-day WRF ensemble members (a-c), future WRF ensemble members (d-f), and the difference between the two (g-i). The counts are number of cells that experienced that rain rate in any ensemble members, normalized by the number of ensemble members. Analysis is limited to values that occur over land in our region of interest. Values greater than 5000 are omitted to allow focus on less frequent higher rain rate values.

distribution. These plots are also useful to show us regions that may have experienced these rain rates multiple times, thus exacerbating impacts (Fig. 8). The heat map for greater than 12.7 mm h^{-1} of rain is presented here, but larger thresholds were also computed (not shown). The largest difference these heat maps reveals is a shift in track between the present ensemble members and the future ensemble members for all storms. Along with the track shift, however, we also see an expansion of the regions experiencing greater than 12.7 mm h^{-1} rain rates (Fig. 8). When we

Table 6. Temporally and spatially averaged changes in atmospheric layer temperature (surface-500 hPa) and precipitable water calculated from the present-day ensemble mean files. Mean hourly rain rates and standard deviations are calculated from all of the ensemble members for each storm. The percent changes are calculated from the ensemble member means and ensemble member 90th percentile precipitation calculations. The plus or minus error metrics represent one standard deviation.

	Matthew (2016)	*Florence* (2018)	*Floyd* (1999)
Temperature change	+4.5K	+4.5K	+4.5K
Expected CC scaling	35%	36%	36%
Present PWAT	40.9 mm	45.3 mm	43.6 mm
Future PWAT	54.2 mm	58.1 mm	57.4 mm
PWAT percent change	32%	28%	31%
Present mean rain rate	11.6 ± 0.4 mm h^{-1}	9.2 ± 0.7 mm h^{-1}	12.1 ± 0.8 mm h^{-1}
Future mean rain rate	14.3 ± 1.2 mm h^{-1}	12.3 ± 0.7 mm h^{-1}	14.6 ± 1.1 mm h^{-1}
Mean rain rate %	23 ± 9%	34 ± 12%	21 ± 6%
90th percentile rain rate %	37 ± 7%	55 ± 20%	25 ± 8%

average the amount of grid cells in which the frequency of rain rates exceeds 12.7 mm h^{-1}, we find increases of 20%, 28%, and 28% for Hurricanes Matthew, Florence, and Floyd respectively. When we average the highest 5% of these frequency values, which gives an idea of how much the area of repeated rain rate occurrence changes at a given threshold, the percent increases are 17%, 47%, and 21% for Hurricanes Matthew, Florence, and Floyd respectively. These precipitation quantities can be useful to planners and state agencies as it gives insight into another potential cause of flooding or flash-flooding: changes in the duration of high-intensity rain rates.

d. Storm-Centered Precipitation Changes

Because of present to future track shifts, it is useful to consider storm-centered precipitation changes by computing the distance from the TC center where the highest rain rates are occurring,

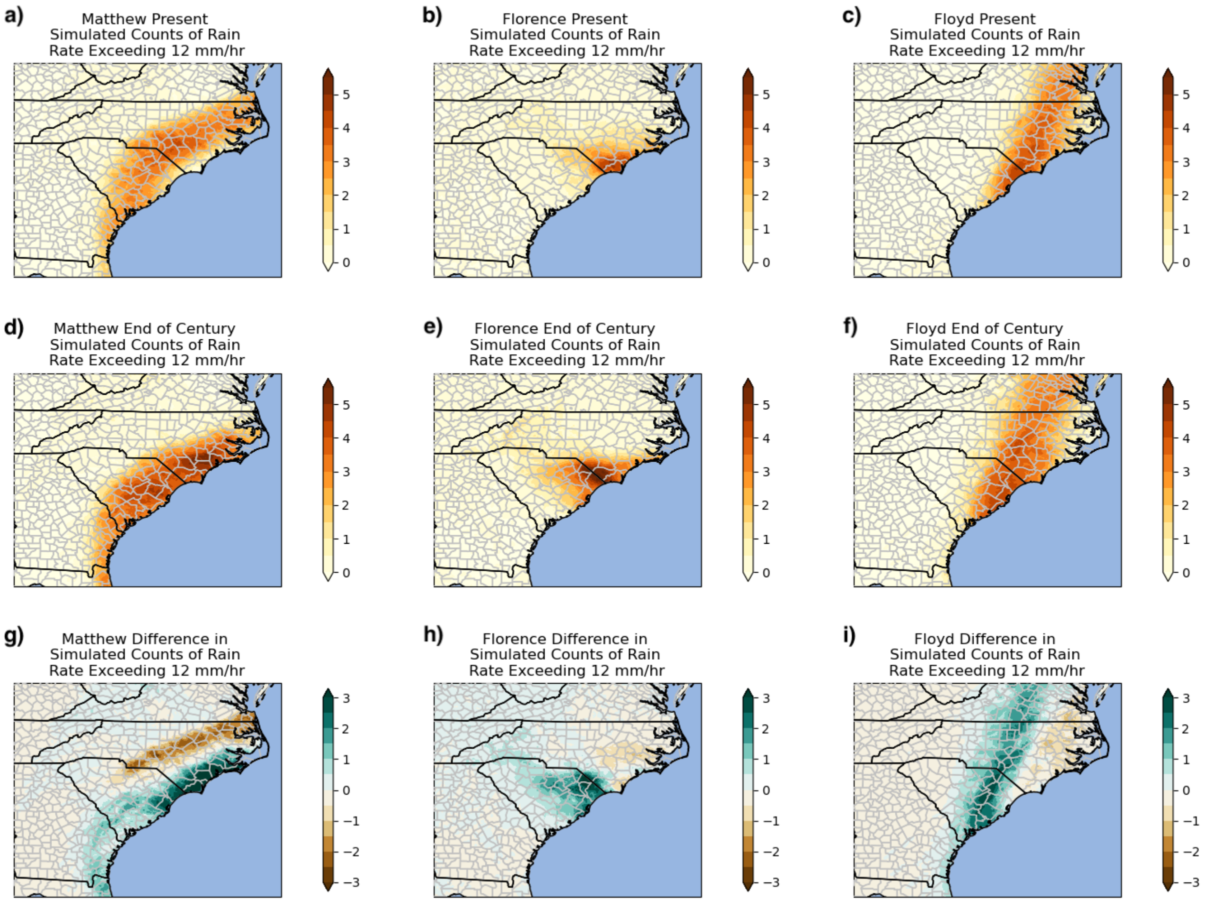

Figure 8. Heatmap of instances of rain rates greater than 12.7 mm h^{-1} occurring in each grid cell, normalized by the number of ensemble members and the number of days in the simulation to allow for a better comparison between storms. Organized as in Fig. 7

and examining how that shifts. As has been shown in previous TC and ET literature (Atallah et al. 2007; Liu et al. 2018; Jung and Lackmann 2019, 2021), TCs with more tropical characteristics exhibit the highest rain rate increases near the TC center; then, as the storm begins to undergo ET, the region of maximum rain rates extends outward away from the TC center. Since our storms are in various stages of ET when they impact North Carolina, we evaluate where the maximum rain rates exist in relation to the distance from the TC center, and how that changes with warming. To do this, we calculated the azimuthal average rain rate values for all of our storms across all simulation times (not shown) and then averaged across the simulation time (including times from both before and after extratropical transition) (Fig. 9). For the storm that most strongly retained tropical characteristics, Florence, we find that in the future the largest rain rate increase of ~110% occurs between 50 and 100 km from the storm center. For Matthew, which was closest to transition while it was impacting the Carolinas, we see the largest increase in rain rates further from the TC center, between 100 and 150 km. The mean magnitude of this difference is an increase of ~90% from present to future. Floyd, which exhibited both tropical and extratropical characteristics when its rain bands were over South and North Carolina, exhibits a double peak: the first within 50 km and the second between 100 and 150 km. The magnitudes of these increases peak at about 50% and 30%, respectively. Both the highest simulated mean rain rates and the largest percent increases in rain rates from present to future were associated with Hurricane Florence. While the magnitude of the changes differ, we find that rain rate increases within 100 and 300 km for our tropical and transitioning storms are super-Clausius Clapeyron; this aligns with the findings in Jung and Lackmann (2021, 2023).

The values presented in Figure 9 are for rain rates that occurred over ocean and land in our Carolinas averaging box; if we instead consider the whole 4-km domain that our storms moved through (not shown), we find that all storms have a rain rate peak within 100 km of the center (as Florence does in Fig. 9) and Matthew and Floyd exhibit a second rain rate peak between 100 and 200 km radial distance. The largest rain rates and the largest increase in rain rates are in future Hurricane Floyd within 75 km of the storm center. While this provides context to the tropical and extratropical-transitioning nature of the full life cycle of these storms, our area of primary interest is the Carolinas, where Florence was tropical and Floyd and Matthew were being influenced by baroclinic systems.

e. Changes in return period of precipitation

The return period can be used to quantify extreme precipitation events in the context of historical events. Here, we quantify the return period for all three storms for different precipitation time intervals (1-hr, 2-hr, 3-hr, 6-hr, 12-hr, and 24-hr; Fig. 10). For all cases, the future storms had a higher return period (e.g., from 100-yr to 500-yr) than the present-day version for all time intervals. At the shorter time intervals, Hurricanes Matthew and Florence exhibit the largest increases in maximum rain rate, with future Matthew exhibiting larger values than Florence at all times shown. When we consider the longer time intervals (i.e. 12-hr and 24-hr), we find that

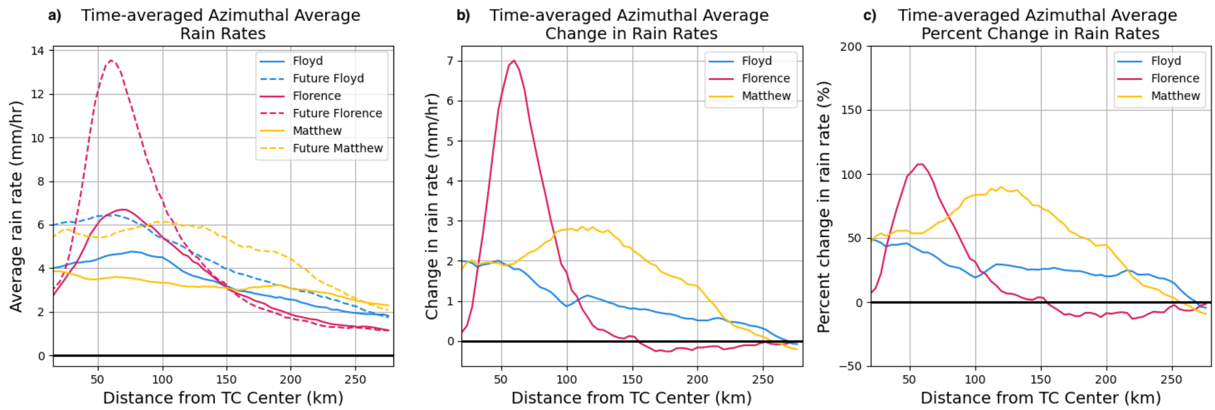

Figure 9. Time mean azimuthal average rain rates as a function of radial distance for Hurricanes Matthew, Florence, and Floyd for the present and future ensemble mean (a); difference between each storm's present and future (b); and percent change in rain rates (c). These values are for rain rates that occurred over the land and ocean in the averaging area over the Carolinas shown in Fig. 4.

Hurricane Florence has larger increases - this is not surprising as Hurricane Florence was a much longer duration storm than either Matthew or Floyd.

When we consider all of these precipitation values in the context of the climate-model (LOCA) adjusted Atlas-14 data, all storms in the present and future and at each rainfall duration period shift to lower return intervals (i.e. if we consider 50, 100, 500, and 1000 year return periods, they shift from 500 to 50 or 1000 to 100 when comparing with historical versus LOCA). Even with these adjustments, however, future Florence and future Matthew are still greater than 1000 year events for all six time intervals we consider here. This speaks to just how rare these storms were historically, and how in a future scenario they can become more frequent but still have even more extreme precipitation. However, this also may suggest that LOCA fails to fully represent TC precipitation, and that what appears here to be a 1000-year event may not be quite as rare.

5. Conclusions

Tropical cyclone rain rates are expected to increase as the climate continues to warm, but the extent of that increase and how it may differ for TCs at different stages in their life cycle, or in contrasting synoptic environments, is less clear. Here, by evaluating over-land rain rate characteristics of three Atlantic TCs at various stages of their life cycles, in diverse synoptic patterns, and in altered climate conditions, we find that there is strong variability amongst the three storms for multiple

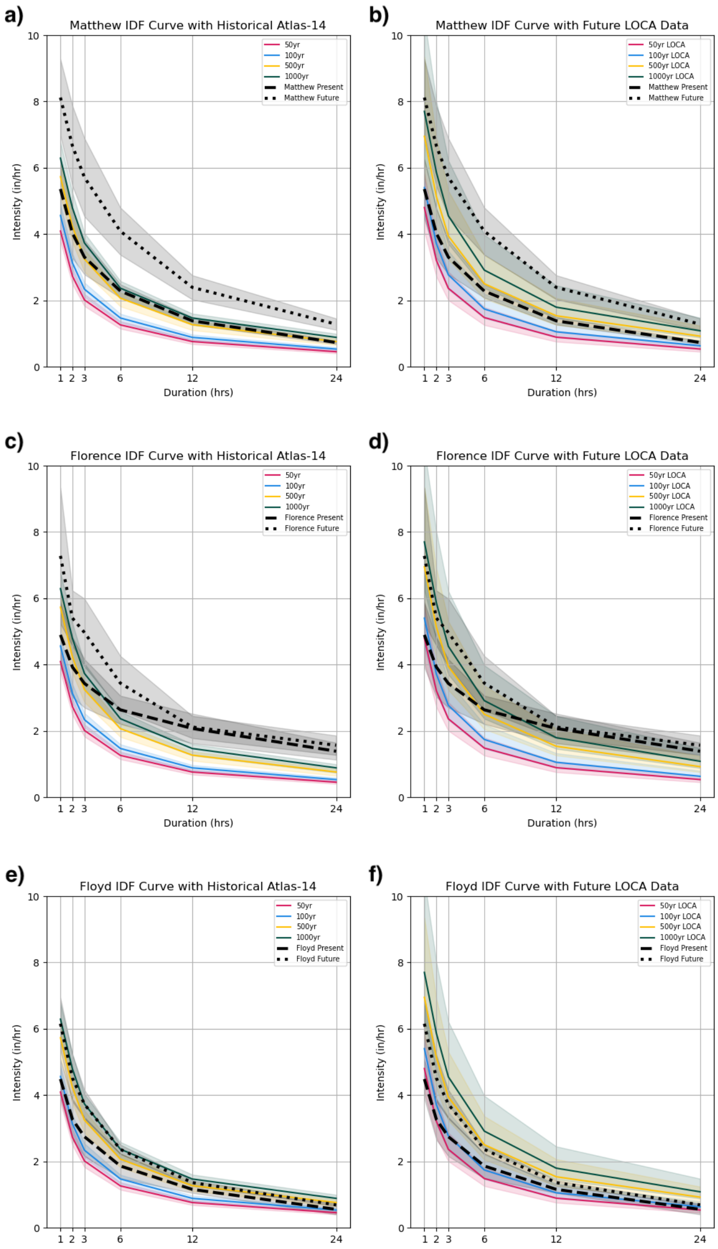

Figure 10. Intensity Duration Frequency curves for historical Atlas-14 values for the New Hanover County station in eastern North Carolina (a, c, e) and for the updated, end-of-century values which include the climate signal from LOCA statistically downscaled climate data (b, d, f). The curves shown represent the 50, 100, 500, and 1000 year return period values for 1, 2, 3, 6, 12, and 24 hour time periods. They represent the average and standard deviation for the 100 highest rain rate values for Hurricanes Matthew (a, b), Florence (c, d), and Floyd (e, f) from the present simulations (dashed line) and future simulations (dotted line).

rainfall characteristics: accumulated rain, distribution of rain rates, spatial distribution of rain rates, and historical extremity of rain rates. We evaluated these three synoptically diverse TC events using high-resolution ensembles in the current climate, and for a high-emission end-of-century thermodynamic environment (RCP 8.5 and SSP585). The main results for changes in each precipitation characteristic are as follows:

- For storm-total accumulated rainfall, the area receiving at least 250mm of rainfall expanded by $17600 \pm 800 km^2$, $9800 \pm 500 km^2$, and $22400 \pm 400 km^2$ for Hurricanes Matthew, Florence, and Floyd, respectively - Hurricanes Matthew and Floyd had almost double the areal expansion of Florence. The largest areal expansions for each storm occurred above a 375 mm threshold for Matthew, 375 mm for Florence, and 250 mm for Floyd.

- When considering how the rain rates changed for each storm, we see an increase in all rain rates greater than 5 mm h^{-1} for each storm, and a decrease in the rain rates below that threshold. We also find that, while Matthew and Floyd have higher average rain rates in the present and future, Florence has the highest percent increase in both the average rain rates and 90th percentile rain rates ($34 \pm 12\%$ and $55 \pm 20\%$).

- Each storm exhibits a greater than 19% increase in the areal coverage of over-land rain rates greater than 12.7 mm h^{-1}, and a greater than 17% increase in the number of hours during which those rain rates occurred. The largest increases in both of these metrics exist with Hurricane Florence (28% and 47% respectively).

- A discernible difference between precipitation metrics for these storms emerges when we consider time-averaged rain rates as a function of distance from the TC center. For Hurricane Florence, a storm that strongly retained tropical characteristics, the highest values and the largest change in rain rate occur within 100 km of the center. Matthew and Floyd, both transitioning storms interacting with synoptic features, exhibited peak rain rates further from the TC center at distances greater than 100 km. Both the highest rain rate of any storm and the largest increase in mean rain rate occurred with Hurricane Florence.

- Each of our future storms was greater than a 100-year return period event for multiple rainfall periods when considering both the historical Atlas-14 scale as well the LOCA-adjusted Atlas-14 that accounts for climate change. Hurricane Matthew's 1-hr, 2-hr, 3-hr, and 6-hr future maximum rain rates were the highest out of all three storms, while Florence had the highest future maximum rain rates for 12-hr and 24-hr duration.

The ensemble of present-day and future simulations can be used to assess future threats, for example to transportation infrastructure. For such applications, where highly localized present-to-future comparisons are needed, a “scale factor” approach is useful because it eliminates challenges created by the shifts in the simulated spatial precipitation distribution. For such applications, we recommend computing precipitation change statistics from the present-day and future ensembles to determine scale factors, such as the percent changes we calculated from the histograms here. Then, the scale factor can be applied to either observed or simulated present-day precipitation. For more on this approach, see Grimley et al. (2024). This scale-factor approach can be modified to consider different storm types, different percentile thresholds, or different regions.

The configuration of this study has a few limitations, one of which is the use of spectral nudging. Two of these storm simulations utilized nudging to encourage the storms to follow similar tracks in the present and the future. Given that nudging constrains track changes, these simulations should not be used to add to the conversation about shifts in future storm tracks. Nudging also reduces environmental changes that may have impacted the resulting precipitation fields, though only the large-scale steering flow was nudged in an attempt to minimize this influence.

Another limitation of this study is the limited sample size of storms studied; only three storms are compared, all of which are relatively modest in intensity and only represent a subset of synoptic environments. We also are only examining one future scenario (RCP8.5) out of many, and one future time period out of many (end of century). While we acknowledge that three storms in one future scenario is not sufficient to fully generalize future TC rainfall changes for storms in a large variety of synoptic settings, and a larger catalog of storms would be preferred in order to represent the variability, there are still some patterns we can identify from our subset of storms. One such pattern is that, while Hurricanes Floyd and Matthew have larger average rain rates in the present and future than Florence (when considering the whole distribution of rain rates), we find the largest percent increases in average rain rate with Hurricane Florence. When we consider these rain rate changes as a function of distance from the TC center, we see that again the largest percent increases in average rain rates exist with Hurricane Florence within 100-km of the storm center. However, Hurricane Florence also has a much smaller areal increase in total accumulated precipitation than both Matthew and Floyd when we consider totals above 250 mm. These findings may point to a difference in climate change response for more tropical, non-synoptic TC rainfall as compared to more extratropical-transitioning, synoptic-interacting TCs. In a subsequent paper, the forcing mechanisms for these precipitation changes will be evaluated to understand what thermodynamic and dynamic mechanisms are contributing to these discrepancies in TC precipitation changes by synoptic environment.

Each of these storms produced substantial rainfall when they occurred historically, and the changes described above indicate that when similar storms occur in a future, warmer climate, the impacts could be even more devastating. We also highlight the importance of evaluating these precipitation changes as a function of the TC environment. It is important to understand how TC rainfall, evaluated from multiple different lenses at different spatial scales, may change as the climate continues to warm in order to help inform infrastructure planning, as well as to assist in attempts to mitigate damage and loss of life caused in the wake of these destructive TCs.

Acknowledgments. This research was supported by the North Carolina Department of Transportation project 2020-57, awarded to North Carolina State University (NCSU), and North Carolina State University. We acknowledge the support of NCDOT Hydraulics Engineer, Matthew Lauffer. High-performance computing support was provided by the North Carolina State University Henry2 and Hazel clusters. Thanks to Chunyong Jung for obtaining and interpolating the CMIP5 GCM data and providing the interpolation codes, and to Brett Roberts (CIWRO) for code and assistance with calculating probability matched mean precipitation. We also thank Lauren Grimley and Lauren Getker for feedback on an earlier version of the manuscript, and Walter Robinson and Anantha Aiyyer for feedback on material for this manuscript.

Data availability statement. The source code for the model used in this study, WRF 4.2.2, is freely available from `https://github.com/wrf-model/WRF/releases?page=2`. Model output from the simulations presented in this manuscript are available at `https://doi.org/10.5061/dryad.x95x69pt8`. ECMWF 5 reanalysis data can be obtained from `https://cds.climate.copernicus.eu/cdsapp#!/dataset/reanalysis-era5-pressure-levels?tab=form`, CFSR data can be obtained from `https://www.ncei.noaa.gov/data/climate-forecast-system/access/`

reanalysis/6-hourly-by-pressure-level/, and GDAS/FNL data can be obtained from https://rda.ucar.edu/datasets/ds083.3/dataaccess/#.

References

Atallah, E., L. F. Bosart, and A. R. Aiyyer, 2007: Precipitation distribution associated with landfalling tropical cyclones over the eastern united states. *Mon. Wea. Rev.*, **135**, 2185–2206, https://doi.org/10.1175/MWR3382.1.

Atallah, E. H., and L. F. Bosart, 2003: The extratropical transition and precipitation distribution of hurricane floyd (1999). *Mon. Wea. Rev.*

Baulenas, E., G. Versteeg, M. Terrado, J. Mindlin, and D. Bojovic, 2023: Assembling the climate story: use of storyline approaches in climate-related science. *Global Challenges*, 2200183.

Bieli, M., A. H. Sobel, S. J. Camargo, H. Murakami, and G. A. Vecchi, 2020: Application of the cyclone phase space to extratropical transition in a global climate model. *Journal of Advances in Modeling Earth Systems*, **12 (4)**, e2019MS001 878, https://doi.org/https://doi.org/10.1029/2019MS001878.

Bonnin, G. M., D. Martin, B. Lin, T. Parzybok, M. Yekta, and D. Riley, 2004: Precipitation-frequency atlas of the united states. volume 2 version 3.0. delaware, district of columbia, illinois, indiana, kentucky, maryland, new jersey, north carolina, ohio, pennsylvania, south carolina, tennessee, virginia, west virginia. Tech. rep., U.S. Department of Commerce.

Bowden, J. H., K. E. Kunkel, G. M. Lackmann, K. Hollinger Beatty, K. Dello, A. M. Jalowska, T. L. Spero, and M. Lauffer, 2025: An apples-to-apples comparison of downscaling methods to inform and produce future precipitation intensity-duration-frequency curves for resilient transportation within north carolina, in preparation.

Bowden, J. H., T. L. Otte, C. G. Nolte, and M. J. Otte, 2012: Examining interior grid nudging techniques using two-way nesting in the wrf model for regional climate modeling. *Journal of Climate*, **25 (8)**, 2805–2823.

Bowden, J. H., and Coauthors, 2024: A comparison of downscaling methods to create future precipitation intensity-duration-frequency curves for resilient transportation within north carolina. *104th AMS Annual Meeting*, AMS.

Carroll-Smith, D., R. J. Trapp, and J. M. Done, 2020: Exploring inland tropical cyclone rainfall and tornadoes under future climate conditions through a case study of hurricane ivan. *J. Appl. Meteor. Climatol.*, **60**, 103–118, https://doi.org/10.1175/JAMC-D-20-0090.1.

Colle, B. A., 2003: Numerical simulations of the extratropical transition of floyd (1999): Structural evolution and responsible mechanisms for the heavy rainfall over the northeast united states. *Mon. Wea. Rev.*

Donelan, M., B. K. Haus, N. Reul, W. Plant, M. Stiassnie, H. Graber, O. B. Brown, and E. Saltzman, 2004: On the limiting aerodynamic roughness of the ocean in very strong winds. *Geophysical Research Letters*, **31 (18)**.

Dougherty, E., and K. L. Rasmussen, 2020: Changes in future flash flood–producing storms in the united states. *J. Hydrometeor.*, **21**, 2221–2236, https://doi.org/10.1175/JHM-D-20-0014.1.

Dougherty, E. M., A. F. Prein, E. D. Gutmann, and A. J. Newman, 2023: Future simulated changes in central u.s. mesoscale convective system rainfall caused by changes in convective and stratiform structure. *Journal of Geophysical Research: Atmospheres*, **128**, https://doi.org/10.1029/2022JD037537.

Evans, C., and Coauthors, 2017: The extratropical transition of tropical cyclones. part i: Cyclone evolution and direct impacts. *Mon. Wea. Rev.*, **145**, 4317–4344, https://doi.org/10.1175/mwr-d-17-0027.1.

Frei, C., C. Schär, D. Lüthi, and H. C. Davies, 1998: Heavy precipitation processes in a warmer climate. *Geophys. Res. Lett.*, **25**, 1431–1434, https://doi.org/10.1029/98GL51099.

Gidden, M. J., and Coauthors, 2019: Global emissions pathways under different socioeconomic scenarios for use in cmip6: a dataset of harmonized emissions trajectories through the end of the century. *Geoscientific Model Development*, **12 (4)**, 1443–1475, https://doi.org/10.5194/gmd-12-1443-2019.

Grimley, L. G., K. E. Hollinger Beatty, A. Sebastian, S. Bunya, and G. M. Lackmann, 2024: Climate change exacerbates flooding from recent tropical cyclones, in preparation.

Gutmann, E. D., and Coauthors, 2018: Changes in hurricanes from a 13-yr convection-permitting pseudo- global warming simulation. *J. Climate*, **31**, 3643–3657, https://doi.org/10.1175/JCLI-D-17-0391.1.

Hausfather, Z., K. Marvel, G. A. Schmidt, J. W. Nielsen-Gammon, and M. Zelinka, 2022: Climate simulations: recognize the ‘hot model’problem. *Nature*, **605 (7908)**, 26–29.

Hersbach, H., and Coauthors, 2020: The era5 global reanalysis. *Quarterly Journal of the Royal Meteorological Society*, **146 (730)**, 1999–2049.

Hill, K. A., and G. M. Lackmann, 2011: The impact of future climate change on tc intensity and structure: A downscaling approach. *J. Climate*, **24 (17)**, 4644–4661.

Jalowska, A. M., T. L. Spero, and J. H. Bowden, 2021: Projecting changes in extreme rainfall from three tropical cyclones using the design-rainfall approach. *npj Climate and Atmospheric Science*, **4**, https://doi.org/10.1038/s41612-021-00176-9.

Jones, S. C., and Coauthors, 2003: The extratropical transition of tropical cyclones: Forecast challenges, current understanding, and future directions. *Wea. Forecasting*, **18 (6)**, 1052–1092.

Jung, C., and G. M. Lackmann, 2019: Extratropical transition of hurricane irene (2011) in a changing climate. *J. Climate*, **32**, 4847–4871, https://doi.org/10.1175/JCLI-D-18-0558.1.

Jung, C., and G. M. Lackmann, 2021: The response of extratropical transition of tropical cyclones to climate change: Quasi-idealized numerical experiments. *J. Climate*, **34**, 4361–4381, https://doi.org/10.1175/JCLI-D-20-0543.1.

Jung, C., and G. M. Lackmann, 2023: Changes in tropical cyclones undergoing extratropical transition in a warming climate: Quasi-idealized numerical experiments of north atlantic landfalling events. *Geophys. Res. Lett.*, **50**, https://doi.org/10.1029/2022GL101963.

Keller, J. H., and Coauthors, 2019: The extratropical transition of tropical cyclones. part ii: Interaction with the midlatitude flow, downstream impacts, and implications for predictability. *Mon. Wea. Rev.*, **147**, 1077–1106, https://doi.org/10.1175/MWR-D-17-0329.1.

Kilgore, R., and Coauthors, 2019: Applying climate change information to hydrologic and coastal design of transportation infrastructure. Tech. rep.

Kimura, F., and A. Kitoh, 2007: Downscaling by pseudo global warming method. *The Final Report of ICCAP*, **4346**, 463–478.

Knutson, T., and Coauthors, 2020: Tropical cyclones and climate change assessment part ii: Projected response to anthropogenic warming. *Bull. Amer. Meteor. Soc.*, **101**, E303–E322, https://doi.org/10.1175/BAMS-D-18-0194.1.

Knutson, T. R., J. J. Sirutis, M. A. Bender, R. E. Tuleya, and B. A. Schenkel, 2022: Dynamical downscaling projections of late twenty-first-century u.s. landfalling hurricane activity. *Climatic Change*, **171**, 28, https://doi.org/10.1007/s10584-022-03346-7.

Knutson, T. R., J. J. Sirutis, M. Zhao, R. E. Tuleya, M. Bender, G. A. Vecchi, G. Villarini, and D. Chavas, 2015: Global projections of intense tropical cyclone activity for the late twenty-first century from dynamical downscaling of cmip5/rcp4. 5 scenarios. *J. Climate*, **28 (18)**, 7203–7224.

Knutson, T. R., and R. E. Tuleya, 2004: Impact of co 2-induced warming on simulated hurricane intensity and precipitation: Sensitivity to the choice of climate model and convective parameterization. *J. Climate*, **17 (18)**, 3477–3495.

Kourtis, I. M., and V. A. Tsihrintzis, 2022: Update of intensity-duration-frequency (idf) curves under climate change: a review. *Water Supply*, **22 (5)**, 4951–4974.

Kunkel, K., and Coauthors, 2020: North carolina climate science report. Tech. rep., North Carolina Institute for Climate Studies.

Lackmann, G. M., 2013: The south-central u.s. flood of may 2010: Present and future*. *J. Climate*, https://doi.org/10.1175/JCLI.

Lackmann, G. M., 2015: Hurricane sandy before 1900 and after 2100. *Bull. Amer. Meteor. Soc.*, **96**, 547–560, https://doi.org/10.1175/BAMS-D-14-00123.1.

Landsea, C. W., and J. L. Franklin, 2013: Atlantic hurricane database uncertainty and presentation of a new database format. *Mon. Wea. Rev.*, **141 (10)**, 3576–3592.

Liu, M., G. A. Vecchi, J. A. Smith, and H. Murakami, 2017: The present-day simulation and twenty-first-century projection of the climatology of extratropical transition in the north atlantic. *J. Climate*, **30**, 2739–2756, https://doi.org/10.1175/JCLI-D-16-0352.1.

Liu, M., G. A. Vecchi, J. A. Smith, and H. Murakami, 2018: Projection of landfalling-tropical cyclone rainfall in the eastern united states under anthropogenic warming. *J. Climate*, **31**, 7269–7286, https://doi.org/10.1175/JCLI-D-17-0747.1.

Liu, M., L. Yang, J. A. Smith, and G. A. Vecchi, 2020: Response of extreme rainfall for landfalling tropical cyclones undergoing extratropical transition to projected climate change: Hurricane irene (2011). *Earth's Future*, **8**, https://doi.org/10.1029/2019EF001360.

Livneh, B., E. A. Rosenberg, C. Lin, B. Nijssen, V. Mishra, K. M. Andreadis, E. P. Maurer, and D. P. Lettenmaier, 2013: A long-term hydrologically based dataset of land surface fluxes and states for the conterminous united states: Update and extensions. *Journal of Climate*, **26 (23)**, 9384–9392.

Lynch, P., and X.-Y. Huang, 1992: Initialization of the hirlam model using a digital filter. *Mon. Wea. Rev.*, **120 (6)**, 1019–1034.

Mallard, M. S., G. M. Lackmann, and A. Aiyyer, 2013a: Atlantic hurricanes and climate change. part ii: Role of thermodynamic changes in decreased hurricane frequency. *J. Climate*, **26 (21)**, 8513–8528.

Mallard, M. S., G. M. Lackmann, A. Aiyyer, and K. Hill, 2013b: Atlantic hurricanes and climate change. part i: Experimental design and isolation of thermodynamic effects. *J. Climate*, **26 (13)**, 4876–4893.

Michaelis, A. C., and G. M. Lackmann, 2019: Climatological changes in the extratropical transition of tropical cyclones in high-resolution global simulations. *J. Climate*, https://doi.org/10.1175/JCLI-D-19.

Michaelis, A. C., and G. M. Lackmann, 2021: Storm-scale dynamical changes of extratropical transition events in present-day and future high-resolution global simulations. *J. Climate*, **34**, 5037–5062, https://doi.org/10.1175/JCLI-D-20-0472.1.

Miro, M., A. DeGaetano, C. Samaras, K. R. Grocholski, T. López-Cantú, M. Webber, and B. Eck, 2021: Projected intensity-duration-frequency (idf) curve tool for the chesapeake bay watershed and virginia. *website), Northeast Regional Climate Center, available online: https://midatlantic-idf. rcc-acis. org/, last accessed May*, **4**, 2022.

Moss, R. H., and Coauthors, 2010: The next generation of scenarios for climate change research and assessment. *Nature*, **463 (7282)**, 747–756.

National Centers for Environmental Prediction, National Weather Service, NOAA, U.S. Department of Commerce, 2015: Ncep gdas/fnl 0.25 degree global tropospheric analyses and forecast grids. Research Data Archive at the National Center for Atmospheric Research, Computational and Information Systems Laboratory, Boulder CO, URL https://doi.org/10.5065/D65Q4T4Z.

Nolan, D. S., B. D. McNoldy, and J. Yunge, 2021: Evaluation of the surface wind field over land in wrf simulations of hurricane wilma (2005). part i: Model initialization and simulation validation. *Mon. Wea. Rev.*, **149**, 679–695, https://doi.org/10.1175/MWR-D-20-0199.1.

Otte, T. L., C. G. Nolte, M. J. Otte, and J. H. Bowden, 2012: Does nudging squelch the extremes in regional climate modeling? *Journal of Climate*, **25 (20)**, 7046–7066.

Pasch, R. J., T. B. Kimberlain, and S. R. Stewart, 1999: Preliminary report hurricane floyd. Tech. rep., National Hurricane Center.

Peckham, S. E., T. G. Smirnova, S. G. Benjamin, J. M. Brown, and J. S. Kenyon, 2016: Implementation of a digital filter initialization in the wrf model and its application in the rapid refresh. *Mon. Wea. Rev.*, **144 (1)**, 99–106.

Pierce, D. W., D. R. Cayan, and B. L. Thrasher, 2014: Statistical downscaling using localized constructed analogs (loca). *J. Hydrometeor.*, **15 (6)**, 2558 – 2585, https://doi.org/https://doi.org/10.1175/JHM-D-14-0082.1.

Rappaport, E. N., 2014: Fatalities in the united states from atlantic tropical cyclones: New data and interpretation. *Bull. Amer. Meteor. Soc.*, **95 (3)**, 341–346.

Reed, K. A., A. M. Stansfield, M. F. Wehner, and C. M. Zarzycki, 2020: Forecasted attribution of the human influence on hurricane florence. *Science Advances*, **6 (1)**, eaaw9253, https://doi.org/10.1126/sciadv.aaw9253.

Saha, S., and Coauthors, 2010: The ncep climate forecast system reanalysis. *Bull. Amer. Meteor. Soc.*, **91 (8)**, 1015–1058.

Sato, T., F. Kimura, and A. Kitoh, 2007: Projection of global warming onto regional precipitation over mongolia using a regional climate model. *Journal of Hydrology*, **333**, 144–154, https://doi.org/10.1016/j.jhydrol.2006.07.023.

Schär, C., C. Frei, D. Lüthi, and H. C. Davies, 1996: Surrogate climate-change scenarios for regional climate models. *Geophys. Res. Lett.*, **23**, 669–672, https://doi.org/10.1029/96GL00265.

Seneviratne, S. I., and Coauthors, 2023: *Weather and Climate Extreme Events in a Changing Climate*, chap. Climate Change 2021 – The Physical Science Basis, 1513–1766. Cambridge University Press, https://doi.org/10.1017/9781009157896.013.

Skamarock, W., and Coauthors, 2021: A description of the advanced research wrf model version 4.3; no. *NCAR/TN556+ STR*.

Stansfield, A. M., K. A. Reed, and C. M. Zarzycki, 2020: Changes in precipitation from north atlantic tropical cyclones under rcp scenarios in the variable-resolution community atmosphere model. *Geophys. Res. Lett.*, **47**, https://doi.org/10.1029/2019GL086930.

Stewart, S. R., 2017: Hurricane matthew. Tech. rep., National Hurricane Center.

Stewart, S. R., and R. Berg, 2019: Hurricane florence. Tech. rep., National Hurricane Center.

Tokarska, K. B., M. B. Stolpe, S. Sippel, E. M. Fischer, C. J. Smith, F. Lehner, and R. Knutti, 2020: Past warming trend constrains future warming in cmip6 models. *Science Advances*, **6 (12)**, eaaz9549, https://doi.org/10.1126/sciadv.aaz9549.

Trapp, R. J., and K. A. Hoogewind, 2016: The realization of extreme tornadic storm events under future anthropogenic climate change. *J. Climate*, **29**, 5251–5265, https://doi.org/10.1175/JCLI-D-15-0623.1.

von Storch, H., H. Langenberg, and F. Feser, 2000: A spectral nudging technique for dynamical downscaling purposes. *Mon. Wea. Rev.*, **128 (10)**, 3664–3673.

Waldron, K. M., J. Paegle, and J. D. Horel, 1996: Sensitivity of a spectrally filtered and nudged limited-area model to outer model options. *Mon. Wea. Rev.*, **124 (3)**, 529–547.

Wright, D. B., C. D. Bosma, and T. Lopez-Cantu, 2019: Us hydrologic design standards insufficient due to large increases in frequency of rainfall extremes. *Geophysical Research Letters*, **46 (14)**, 8144–8153.

Wright, D. B., T. R. Knutson, and J. A. Smith, 2015: Regional climate model projections of rainfall from u.s. landfalling tropical cyclones. *Climate Dynamics*, **45**, 3365–3379, https://doi.org/10.1007/s00382-015-2544-y.